

Kinetic accessibility of buried DNA sites in nucleosomes

Wolfram Möbius, Richard A. Neher, and Ulrich Gerland

Arnold Sommerfeld Center for Theoretical Physics (ASC) and Center for Nanoscience (CeNS),
LMU München, Theresienstraße 37, 80333 München, Germany
(Dated: July 22, 2019)

We study the dynamics of spontaneous conformational fluctuations in nucleosomes, where the DNA partially unwraps from the histone core to expose sites that are normally buried. Using simulations and theoretical analysis of a coarse-grained model, we determine the dependence of the timescales for site exposure and re-burial on the unwrapped DNA length. The interplay between the dynamics of barrier crossing in the DNA-histone contact potential and the internal polymer dynamics of the DNA introduces a length regime of flexibility-assisted barrier crossing.

Even though the DNA in eukaryotic cells is packaged into chromatin, its genetic information must be accessible to proteins for read out and processing [1]. The structural organization of chromatin is fairly well known: the fundamental packaging unit is a nucleosome core particle (NCP) consisting of about 150 base pairs (bp) of DNA wrapped in 1.7 turns around a cylindrical histone complex [2], and chromatin is an array of regularly spaced NCPs, which form a higher order structure. In contrast, the conformational dynamics of chromatin is poorly understood. Two recent experiments studied these dynamics on the level of individual NCPs [3, 4]. Using single-molecule fluorescence techniques, they directly observed conformational fluctuations where DNA transiently unwraps from the histone. During such ‘windows of opportunity’, proteins can access DNA sites that are buried most of the time. This mode of access, driven by thermal energy, is particularly important for passive DNA-binding proteins such as transcription factors. Here, we study these conformational dynamics theoretically within a physical model, see Fig. 1(a).

Consider a buried DNA site which becomes accessible once a DNA segment of length L unwraps from the histone core. What are the typical timescales for unwrapping and rewinding? And how do these timescales depend on L ? An early theoretical study [5] suggested an all-or-none opening mechanism where the nucleosome fluctuates between two states (DNA either fully wrapped or nearly straight), implying that the timescales should be independent of L . Taken together, the recent experiments suggest instead a significant dependence on L in both timescales: a 30 bp DNA segment requires about 250 ms for unwrapping and remains unwrapped for 10–50 ms [3], whereas a 60 bp DNA segment requires 2–5 s for unwrapping and remains unwrapped for 100–200 ms [4]. These results, like previous biochemical experiments [6], imply a gradual multi-step opening mechanism.

While the absolute timescales reported in [3, 4] depend on microscopic details, the physics of their L -dependence can be investigated with coarse-grained models, similar in spirit to previous theoretical work on histone-DNA interactions which focused mainly on static properties or the calculation of free energy barriers, see e.g. [5, 7, 8].

Here, we study the interplay between the DNA polymer dynamics and the dynamics of breaking and reforming DNA-histone contacts. We show that this interplay introduces a novel characteristic length scale ℓ_c , the physics of which is best understood within a toy model, see Fig. 1(b). The length ℓ_c is shorter than the persistence length ℓ_p and can drastically affect the L -dependence of the experimentally observable timescales for DNA site accessibility. While we study here only the dynamics of isolated NCPs, this length scale will be important also for the dynamics of nucleosome arrays.

Nucleosome model. To describe the polymer properties of nucleosomal DNA, we use a discrete bead-spring model with N beads at positions r_i , connected through a harmonic potential between adjacent beads, $U_{\text{spring}} = "s"_{ij} (r_{i+1} - r_j - a)^2/2$, where “ s ” denotes the spring stiffness and a the typical bead separation. We account for the bending rigidity of DNA by a bending energy $U_{\text{bend}} = "b"_{i,j} (1 - \cos \theta_i)$ with bending stiffness “ b ” and local bending angles θ_i at each bead. Furthermore, we incorporate the (screened) electrostatic self-repulsion of DNA through a Debye-Hückel potential $U_{\text{DH}} = k_B T \lambda_B (a)^2 \sum_{i \neq j} e^{-\lambda_B |r_i - r_j|}$ with the Bjerrum length $\lambda_B = 0.7$ nm, the DNA charge density $\rho = 2$ charges per bp, and the screening length $\lambda_B = 1$ nm at physiological salt conditions.

We derive our model for the DNA-histone attraction from the NCP crystal structure [2], which shows that both the electrostatic and hydrogen bond interactions are mainly localized to 14 contact points where the minor

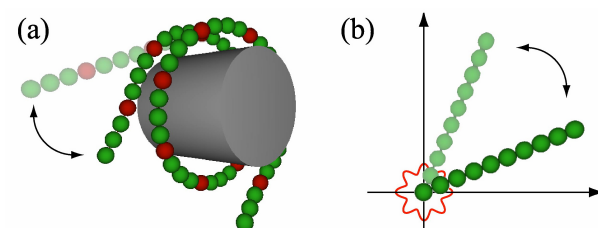


FIG. 1: (a) Illustration of our nucleosome model. The red/dark beads feel a contact potential. (b) Sketch of the Semi-flexible Brownian Rotor (SBR) model.

DNA groove faces the protein core. These contact points lie approximately evenly spaced by 10.2 bp along a superhelical contour with radius 4.2 nm and helical pitch 2.4 nm [8]. Since we are only interested in the dynamics at a fixed (physiological) salt concentration, we combine the electrostatic and hydrogen bond interactions at each of these points into a simple Morse potential, so that the DNA-histone interaction energy takes the form

$$U_{\text{bind}} = \frac{k_B T}{n} \left(1 - e^{-\frac{2\pi}{\lambda} (n - c_i)^2} \right); \quad (1)$$

where the sum is over the contact points c_i and $i(n)$ is the bead bound to contact n in the ground state, see Fig. 1. Taken together, the total energy function U (Fig) for our nucleosome model is $U = U_{\text{spring}} + U_{\text{bend}} + U_{\text{DH}} + U_{\text{bind}}$.

Parameter choice. We use a discretization of $N = 59$ beads (one bead per contact plus 3 beads between contacts and at each end), which corresponds to about 2.5 bp/bead with the given superhelical contour. We adjust λ such that the apparent persistence length matches the known $\lambda_p = 50$ nm for DNA at physiological salt conditions. The stretching stiffness $s = 200 k_B T = \text{nm}^2$ assures that the contour length of the DNA is kept approximately constant. We choose a contact radius of $r = 0.5$ nm, which lies between the range of hydrogen bonds and electrostatic interactions. We then adjust the depth of the potential well so that the minimum free energy cost [9] for opening an additional contact is about $1.5 k_B T$, a value that is compatible with experimental estimates [8, 10]. This leads to $\lambda = 21.7$.

Unwrapping dynamics. To study the dynamics of spontaneous DNA unwrapping and rewinding within our nucleosome model, we perform Brownian dynamics simulations using the overdamped Langevin equations

$$\dot{r}_i(t) = -b r_i U'(r_j) + \eta_i(t); \quad (2)$$

where b is the bead mobility and η_i are random forces correlated according to $\langle \eta_i(t) \eta_j(t') \rangle = 6 k_B T b \delta_{ij} \delta(t - t')$. Starting from the completely wrapped state where all contacts are closed, we determine the average time $\tau_{\text{open}}(n)$ until the n -th contact has opened and the unwrapped DNA segment becomes "accessible" (defined here as reaching a nearly straight conformation). Then we determine the average time $\tau_{\text{close}}(n)$ until the n -th contact recloses, so that the DNA between contacts n and $n + 1$ is no longer accessible. Since the spontaneous unwrapping of long DNA segments is extremely rare, we used the forward flux sampling method [11] to reduce the computational effort for determining $\tau_{\text{open}}(n > 2)$. Fig. 2 shows $\tau_{\text{open}}(n)$ (squares, semi-logarithmic scale) and $\tau_{\text{close}}(n)$ (circles). Note that the absolute timescale in Fig. 2 is shorter than in the experiments [3, 4]. This absolute scale depends on the precise form of the DNA-histone interaction and other microscopic details which are not the focus of this letter. Instead, we now want

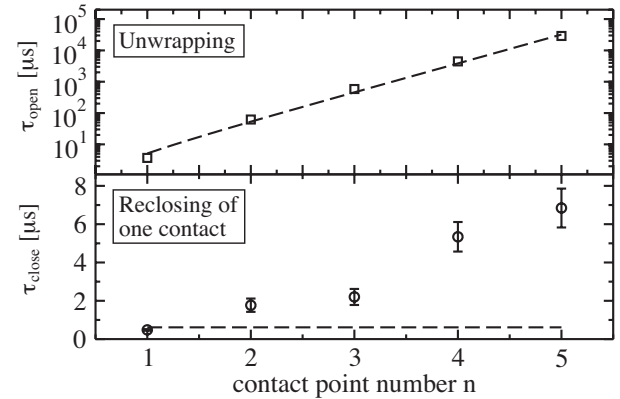


FIG. 2: Brownian dynamics simulations of DNA site exposure. The squares show the average time $\tau_{\text{open}}(n)$ to open the n -th contact point starting from a nucleosome conformation with all contacts closed, while the circles show the average time $\tau_{\text{close}}(n)$ the n -th contact point remains open. The dashed lines result from the minimal model (see main text).

to clarify the physics that governs the functional dependence of the timescales on n .

Test of a minimal description. To interpret our simulations, we first attempt to describe the obtained time scales $\tau_{\text{open}}(n)$ and $\tau_{\text{close}}(n)$ by a minimal model for a gradual, multi-step opening mechanism, i.e. a constant rate for the opening, k_u , and closing, k_b , of consecutive DNA-histone contacts. The ratio $K = k_b/k_u$ then corresponds to the effective equilibrium binding constant per contact. In this model, the average time to open n contacts from one end is the mean first passage time for a 1D biased random walk to reach the n -th site,

$$\tau_{\text{open}}(n) = \frac{k_u^{-1}}{1 - K} \frac{1 - K^n}{1 - K^{-1}} + n \frac{K^{-1} K^n - 1}{k_u}; \quad (3)$$

starting from site zero (reflecting boundary) [12]. The exponential increase of $\tau_{\text{open}}(n)$ is intuitively clear from the fact that the biased random walk is equivalent to a random walk against a free energy ramp. In contrast, the minimal model predicts a constant reclosing time $\tau_{\text{close}}(n) = 1/k_b$. A simultaneous fit of the minimal model to all of the simulation data yields $K = 8.4$ and $k_u = 0.2 = s$, see the dashed lines in Fig. 2. We observe that the unwrapping times are well described by the minimal model (3), whereas a constant $\tau_{\text{close}}(n)$ is clearly not compatible with the simulations.

Polymer effects. The minimal model focuses on the state of the DNA-histone contacts and neglects the dynamics of the DNA. Yet, for a contact to open or close, the loose DNA end must turn by an angle $\theta \approx 45^\circ$, and its rotational mobility clearly decreases with its length L . Since $L \approx \lambda_p$, it seems reasonable to estimate θ by that of a stiff rod, which decreases as L^{-3} [13]. This mobility enters the Kramers rate as a prefactor, implying $\tau_{\text{close}} \propto n^3$. However, $\tau_{\text{close}}(n)$ in Fig. 2 is not compatible

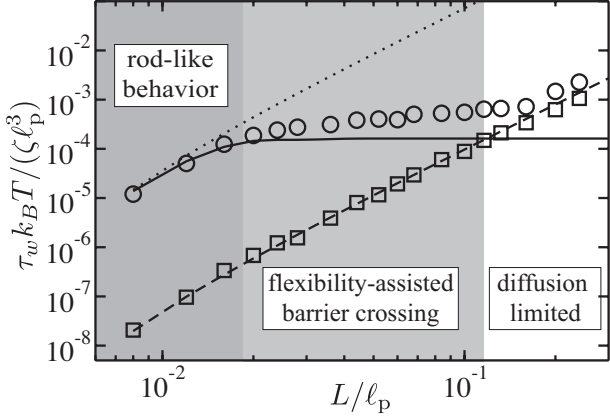


FIG. 3: The average barrier crossing time τ_w (circles) for the SBR model of Fig. 1(b). At small lengths, the barrier crossing time follows that of rigidly connected beads (indicated by the dotted line). However, beyond a certain crossover length ℓ_p , barrier crossing is much faster than for a stiff rod. For large lengths, τ_w approaches the diffusion limit (indicated by squares). Note, that for the length regime $L < \ell_p$ considered here, free diffusion of the SBR is indistinguishable from that of a rigid rod (dashed line). The crossover from the rod-like regime to the intermediate regime is well described by the theoretical analysis described in the main text (solid line).

with a n^3 -behavior, but increases much slower with the length. Our main aim in the following is to show that the internal polymer dynamics can accelerate barrier crossing even for $L > \ell_p$. To the best of our knowledge, barrier crossing of semi-flexible polymers has so far been studied only for situations where the entire polymer experiences an external potential [14]. In the NCP, the action of the potential is on the attachment angle at a single point.

Semi-flexible Brownian Rotor. To examine the coupled dynamics of the internal degrees of freedom and rotational barrier crossing, we introduce a simple model system, the semi-flexible Brownian rotor (SBR): a semi-flexible polymer in two dimensions attached to a point about which it can rotate while the other end is free, see Fig. 1(b). The attachment angle θ experiences a potential $V(\theta) = V_0 \cos(2\theta - \phi)$, leading to preferred attachment angles separated by potential barriers as in our nucleosome model. The main difference is that the length of the rotating polymer is constant in the SBR, while it changes when the DNA is unwrapped in the nucleosome. Also, we do not consider a directional bias in the SBR, since it is not essential for what follows.

Over the scale of many potential wells, the rotational motion of the SBR is diffusive. We express its rotational diffusion coefficient as $D = \langle \dot{\theta}^2 \rangle = 2\tau_w$, where τ_w is the average time to cross one barrier. Since τ_w is related to long-time diffusion, such barrier crossing events involve not only the passage of θ to a neighboring valley in $V(\theta)$, but also the turning of the polymer tip into the direction of the new valley. Hence, τ_w is analogous to the

time scales open and close in our nucleosome model.

The circles in Fig. 3 show τ_w as a function of $L = \ell_p$ obtained with Brownian dynamics simulations for $V_0 = 5 k_B T$. We observe that at very short lengths, τ_w does indeed follow the stiff rod behavior indicated by the dotted line. However, above a certain length ℓ_p , there is a regime where τ_w is nearly insensitive to L , before it rises again. Hence, for lengths $L > \ell_p$ the semi-flexible polymer crosses the barrier much faster than the stiff rod. What is the physical mechanism for this acceleration? One effect of a finite flexibility is a reduced mean end-to-end distance (due to the undulations in the contour), which in turn leads to a larger rotational mobility. However, the free rotational diffusion of a semi-flexible polymer (squares in Fig. 3) is almost identical to that of a stiff rod (dashed line) when $L < \ell_p$. Hence the acceleration is not a mere mobility effect. Note that the dashed line is also the diffusion limit for τ_w , which induces a second crossover from a reaction to a diffusion controlled process.

Flexibility-assisted barrier crossing. To understand the interplay between the polymer dynamics and the barrier crossing dynamics qualitatively, we recall the basic aspects of each: (i) A semi-flexible polymer of length L relaxes its conformational degrees of freedom in a time $L^4 = \ell_p^4$ [15]. Conversely, within a given time τ , a local bending deformation is "felt" only over a length $\ell_p (\tau)^{1/4}$. (ii) The probability current over a barrier is proportional to the quasi-equilibrium occupancy of the transition state and to the relaxation rate τ^{-1} out of this state. Together, (i) and (ii) imply that ℓ_p is the length of the polymer segment that gets deformed during the relaxation process away from the potential peak. We estimate ℓ_p by noting that the attachment angle relaxes according to $\dot{\theta} = -\langle \theta \rangle \partial V / \partial \theta$, where $\langle \theta \rangle \sim \ell_p^3$ is the rotational mobility of the deformed segment. Hence,

$$\dot{\theta} = -\langle \theta \rangle \partial V / \partial \theta = -V_0 \ell_p^3 / \tau, \quad (4)$$

where C is a constant to be determined below. For lengths below ℓ_p , the entire polymer is involved in the relaxation process, i.e. it behaves like a stiff rod.

Quantitative theory for the crossover. To render the above picture quantitative, we employ the Langer theory for multidimensional barrier crossing processes [16]. For the case at hand, one can show [17] that the barrier crossing time simplifies to $\tau_w = -e^{2V_0/k_B T}$, where

λ is the eigenvalue associated with the unstable mode at the saddle point. We calculate λ using the continuous worm-like chain model in the weakly bending approximation [18]. At the transition state the chain is straight, e.g. along the x -axis. We denote deviations from this conformation by $y(x; t)$. The chain dynamics follows $\partial_t y = -\langle \theta \rangle T \partial_x^2 y$ with a friction coefficient $\langle \theta \rangle$. With $\lambda = V_0 (2 - \ell_p^2)^{1/2}$ denoting the curvature of the

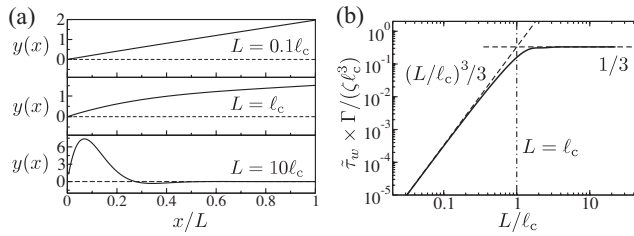


FIG. 4: Dynamics at the barrier. (a) The unstable eigenmode for three different lengths. Polymers shorter than ℓ_c rotate without significant deformation, while long polymers form a bulge of size ℓ_c at the origin. (b) The prefactor of the Kramers time $\tau_w = 1 =$ as a function of the length. The prefactor increases as L^3 if $L \ll \ell_c$ and is constant if $L \gg \ell_c$.

potential at the transition state, the torque on the attached polymer end is $\mathbb{Q}_x y_{j=0}$. This torque must be balanced by a local bend resulting in the boundary condition $k_B T \mathbb{Q}_p^2 y_{j=0} = \mathbb{Q}_x y_{j=0}$. The other boundary conditions are $y_{j=0} = \mathbb{Q}_x^2 y_{j=L} = \mathbb{Q}_x^3 y_{j=L} = 0$. We find a unique unstable mode with eigenvalue $\lambda = k_B T \mathbb{Q}_p^4 = 4 L^4$ and determined by

$$\frac{[\sinh(\lambda) \quad \sin(\lambda)]}{\cosh(\lambda) + \cos(\lambda) + 2} = \frac{\mathbb{Q}_p^2}{12} \frac{L}{\ell_c}; \quad (5)$$

where ℓ_c is as in (4) with $C = \frac{\mathbb{Q}_p^2}{12}$. In the limit $L \ll \ell_c$, we find $\lambda = 3 = L^3$ independent of the stiffness, whereas in the opposite limit $\lambda = 3 = \ell_c^3$ independent of L . Fig. 4 shows (a) the unstable eigenmode for $L = \ell_c = 10$, 100 , and (b) the crossover in the barrier crossing time. The eigenmode shape confirms our qualitative picture: stiff and short polymers respond to the torque by rotating as a whole, whereas the torque shapes a bulge of size ℓ_c in longer polymers. For a discrete polymer model, the same analysis can be performed, but the eigenvalue λ must be computed numerically. The solid line in Fig. 3 shows the resulting barrier crossing time for the same discretization as used in the Brownian dynamics simulations of the SBR model. Indeed, the crossover from the rod-like to the flexibility-assisted barrier crossing is well described by this analysis. The deviations at larger L can be attributed to finite barrier corrections [19].

Discussion and Outlook. Single-molecule experiments on NCPs indicate that the timescales for DNA site accessibility depend on how much DNA needs to be unwrapped [3, 4]. Here, we studied this dependence within a physical model and identified an intricate interplay between the dynamics of the histone-DNA interactions and the polymer dynamics of DNA. This interplay introduces the lengthscale (4) in addition to the lengthscales L and ℓ_p , which govern the dynamics of a free semistiff polymer [15]. The length scale ℓ_c is associated with a striking effect, a flexibility-induced acceleration of barrier crossing events that we have studied in detail within our SBR

model, see Fig. 3, and that arises similarly during DNA (un)wrapping in our nucleosome model. One can interpret ℓ_c as the length over which the contour is deformed as it passes over the potential barrier. Depending on the barrier size, ℓ_c can be much shorter than the persistence length and may probe polymer-specific properties. Our predictions can be tested by additional experiments of the type of [3, 4], but for different unwrapping lengths. Alternatively, one could use DNA of > 150 bp to vary the length of the free DNA ends. Indeed, the presence of linker DNA and the attached neighboring NCPs *in vivo* will significantly affect the absolute timescales of DNA (un)wrapping. However, we expect that the flexibility-induced acceleration effect and the lengthscale ℓ_c will remain relevant.

It is a pleasure to thank H. Boroudjerdi, T. Franosch, E. Frey, O. Hallatschek, S. Leuba, R. Netz, R. Phillips, P. R. ten Wolde, and J. Widom for useful discussions. UG acknowledges an Emmy Noether Grant of the DFG.

- [1] K. Luger and J.C. Hansen, *Curr. Opin. Struct. Biol.* **15**, 188 (2005).
- [2] K. Luger et al., *Nature* **389**, 251 (1997).
- [3] G. Li, M. Levitus, C. Bustamante, and J. Widom, *Nat. Struct. Mol. Biol.* **12**, 46 (2005).
- [4] M. Tomschik, H. Zheng, K. van Holde, J. Zlatanova, and S. Leuba, *Proc. Natl. Acad. Sci. USA* **102**, 3278 (2005).
- [5] N. L. Marky and G. S. Manning, *J. Mol. Biol.* **254**, 50 (1995).
- [6] K. Polach and J. Widom, *J. Mol. Biol.* **254**, 130 (1995).
- [7] K. Kunze and R. Netz, *Phys. Rev. Lett.* **85**, 4389 (2000); I. Kulic and H. Schiessel, *Phys. Rev. Lett.* **91**, 148103 (2003); *ibid.* **92**, 228101 (2004); W. Li, S.-X. Dou, and P.-Y. Wang, *J. Theor. Biol.* **230**, 375 (2004); D. Beard and T. Schlick, *Structure* **9**, 105 (2001).
- [8] H. Schiessel, *J. Phys.: Condens. Matter* **15**, 699 (2003).
- [9] Note that our free energy cost per contact is slightly larger for the first contact and considerably larger when less than one turn of the superhelix remains wrapped, due to the electrostatic self-repulsion of DNA.
- [10] J. Widom, *Q. Rev. Biophys.* **34**, 269 (2001).
- [11] R. J. A llen, D. Frenkel, and P. R. ten Wolde, *J. Chem. Phys.* **124**, 024102 (2006).
- [12] C. Gardiner, *Handbook of Stochastic Methods* (Springer-Verlag, Berlin, 1983).
- [13] M. Doi and S. Edwards, *The theory of polymer dynamics* (Clarendon Press, Oxford, 1986).
- [14] P. Krajcik, R. Lipowsky, and J. Kierfeld, *Europhys. Lett.* **66**, 763 (2004).
- [15] L. Le Go, O. Hallatschek, E. Frey, and F. Ambjörn, *Phys. Rev. Lett.* **89**, 258101 (2002).
- [16] J. Langer, *Phys. Rev. Lett.* **21**, 973 (1968).
- [17] W. Moebius, R. A. Neher, and U. Gerland, *in preparation*.
- [18] see e.g. C. Wiggins, D. R. Kiveline, A. Ott, and R. E. Goldstein, *Biophys. J.* **74**, 10431060 (1998).
- [19] P. Talkner, *Chem. Phys.* **180**, 199 (1994).